Low-lying fermion modes, topology, and light hadrons in quenched QCD

Thomas DeGrand and Anna Hasenfratz
Department of Physics, University of Colorado, Boulder, Colorado 80309
(Received 21 December 2000; published 10 July 2001)

We explore the properties of low lying eigenmodes of fermions in the quenched approximation of lattice QCD. The fermion action is a recently proposed overlap action and has exact chiral symmetry. We find that chiral zero-eigenvalue modes are localized in space and their positions correlate strongly with the locations (as defined through the density of pure gauge observables) of instantons of the appropriate charge. Nonchiral modes are also localized with peaks that are strongly correlated with the positions of both charges of instantons. These correlations slowly die away as the fermion eigenvalue rises. Correlators made of quark propagators restricted to these modes closely reproduce ordinary hadron correlators at small quark mass in many channels. Our results are in qualitative agreement with the expectations of instanton liquid models.

DOI: 10.1103/PhysRevD.64.034512 PACS number(s): 11.15.Ha, 12.38.Aw, 12.38.Gc

I. INTRODUCTION

Is there a particular physical mechanism in QCD that is responsible for chiral symmetry breaking? If so, what other qualitative or quantitative features of QCD depend on this mechanism? The leading candidate for the source of chiral symmetry breaking is topological (instanton) excitation of the gauge field, which couples to the quarks through the associated fermion zero modes (or near-zero modes, after mixing) leading to chiral symmetry breaking via the Banks-Casher [1] relation. An elaborate phenomenology built on the interactions of fermions with instantons is said to account for many of the low energy properties of QCD (for a review, see Refs. [2,3]).

Lattice simulations can in principle address this issue, and indeed this is a large and active area of research. However, nearly all results, be they from pure gauge operators or from fermions, are contaminated by one kind of lattice artifact or another, which clouds the picture.

The problem is that, typically, pure gauge topological observables depend on the operator used. The dominant features of the QCD vacuum seen in any lattice simulation are just ultraviolet fluctuations, as they would be for any quantum field theory. To search for instantons (or other objects), one must invent operators that filter out long distance structure from this uninteresting noise. Some quantities [such as the topological susceptibility in $SU(3)$ gauge theory] are less sensitive to filtering, but some (such as the size distribution of topological objects) are more so, and most results are controversial (see Ref. [4] for a recent summary).

Perfect action topological operators [5,6] offer a mathematically consistent definition for the pure gauge topological charge, but the implementation of such an operator is prohibitively expensive for QCD. Even if there is a pure gauge definition of topology, the situation is still that what is important is what the fermions experience. Here the problem is that until recently, all lattice fermion actions were contaminated by chiral-symmetry sensitive artifacts. The dimension-5 operator which eliminates doubling in Wilson-type actions breaks chiral symmetry and spreads the real eigenmodes of the Dirac operator over a finite range, making the connection between what would otherwise be zero modes and instantons problematic. In principle, even domain wall fermions at finite values of the fifth dimension would show similar artifacts (although in practice they are much reduced). Staggered fermions generally do not have zero eigenmodes in the presence of instantons [7]: the modes split into imaginary pairs and one must try to separate the pairs that would be zero modes from the true non-chiral eigenmodes. At small lattice spacing the chiral symmetry breaking problems are reduced and some studies seem to grapple successfully with lattice artifacts, but the whole situation is rather unsatisfactory [8].

The discovery of lattice actions that implement an exact chiral symmetry without doubling [9] allows one to revisit these questions in a theoretically clean context. One explicit realization of such an action is the overlap action of Neuberger [10]. It obeys the simplest version of the Ginsparg-Wilson [11] relation. So far there have been many studies of aspects of quenched QCD with overlap actions built from the usual Wilson fermion action in four dimensions [12–19]. The results we will present here are based on a new overlap action recently described by one of us [20].

The advantage of studying questions relevant to chiral symmetry on the lattice with an overlap action is obvious: the action itself is chiral. Real-eigenvalue eigenmodes of the Dirac operator are true chiral zero modes. No fine tuning of parameters or post-processing of lattice data is required to do measurements at or close to the chiral limit. All analysis becomes much simpler.

The main disadvantage of the overlap is its expense: for the action of Ref. [20], about a factor of 100 more costly than the clover action to do any calculation that can be done with the clover action. However, overlap calculations can be used to ''validate'' simpler measuring techniques on smaller lattices, and the simpler techniques can then be used to make measurements on large lattices.

In this paper we study the low lying eigenmodes of an overlap action. We observe that these modes show a spatially peaked structure: chiral zero modes correlate with the positions of the appropriately charged topological objects while nonchiral modes correlate with the positions of both signs of topological charge. Next we show that, when the quarks are sufficiently light, these eigenmodes contribute in an impor-

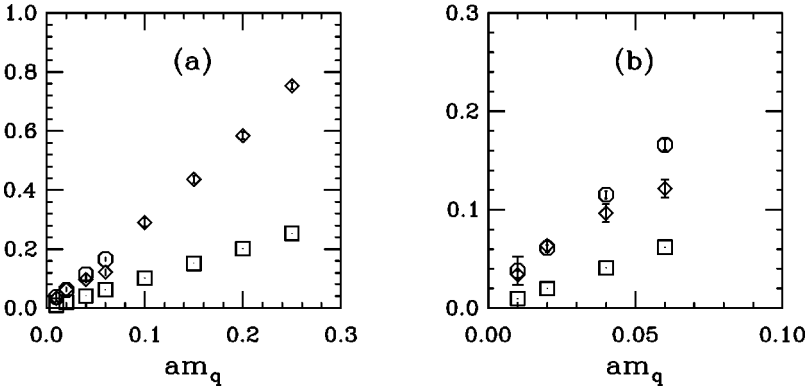

FIG. 1. Squared pion mass (diamonds and octagons) and quark mass from the PCAC relation (squares) from the planar overlap action. Panel (b) merely blows up the small quark mass data of panel (a). The four lighter mass values are from the $12^3\times 24$ lattices. Diamonds show pion masses extracted from a fit to the pseudoscalar-pseudoscalar correlator, and octagons show the pion mass extracted from a fit to the difference of the pseudoscalar-pseudoscalar and scalar-scalar correlators. See Sec. IV for further discussion.

tant way to ordinary hadron correlators (as used, for example, in a spectroscopy calculation), just as the instanton phenomenology would expect them to do. As the quark mass grows heavier, these modes become less important even though manifestations of chiral symmetry breaking persist in spectroscopy and matrix elements.

The study of topology most similar to ours is the investigation of the deconfined phase of $SU(2)$ gauge theory by Edwards *et al.* [15].

In Sec. II we give a brief summary of our simulations, and then in Sec. III we describe our observations of the properties of low-lying eigenmodes of the Dirac operator. In Sec. IV we examine the relevance of these modes to hadronic correlators. We summarize our results in Sec. V.

II. SIMULATION PARAMETERS

The overlap action used in these studies [20] is built from an action with nearest and next-nearest neighbor couplings. The action uses APE-blocked links [21]: Our definition of this blocking is

$$V_\mu^{(n)}(x)=Proj_{SU(3)}\Big\{(1-\alpha)V_\mu^{(n-1)}(x)+(\alpha/6)\times\sum_{\nu\neq\mu}[V_\nu^{(n-1)}(x)V_\mu^{(n-1)}(x+\hat{\nu})V_\nu^{(n-1)}(x+\hat{\mu})^\dagger+V_\nu^{(n-1)}(x-\hat{\nu})^\dagger V_\mu^{(n-1)}(x-\hat{\nu})\times V_\nu^{(n-1)}(x-\hat{\nu}+\hat{\mu})]\Big\}, \tag{1}$$

with $V_\mu^{(n)}(x)$ projected back onto $SU(3)$ after each step, and $V_\mu^{(0)}(n)=U_\mu(n)$ the original link variable. Here we chose $\alpha=0.45$ and performed 10 smearing steps. The massive overlap Dirac operator for bare quark mass m will be denoted as $D(m)$. Eigenmodes of the massless overlap Dirac operator $D(0)$ are constructed from eigenmodes of the massless Hermitian Dirac operator $H(0)=\gamma_5 D(0)$, using an adaptation of a conjugate gradient algorithm of Bunk *et al.* and Kalkreuter and Simma [22]. The code makes extensive use of multimass conjugate gradient matrix inverters [23].

The data set used in this analysis uses the Wilson gauge action at a coupling $\beta=5.9$, or a nominal lattice spacing of $a\simeq 0.11$ fm. It consists of 20 12^4 configurations and 20 $12^3\times 24$ configurations. Data collection took about three months on the Colorado 29 (give or take a few) node Beowulf cluster.

We have done an exploratory spectroscopy calculation on these data sets, at four values of the light quark mass. We also computed the spectrum at four heavier quark masses on the 12^4 set. We show two sets of results, simply to demonstrate how un-exceptional our measurements are. Figure 1 shows the squared pion mass (from two correlators). The ratio of the axial vector ($A_0=\bar{\psi}\gamma_0\gamma_5\psi$) matrix element to the pseudoscalar ($P=\bar{\psi}\gamma_5\psi$) matrix element gives the so-called PCAC (partial conservation of axial vector coupling) quark mass (in lattice regularization)

$$2m_q=\frac{\sum_{\vec{y}}\langle\partial_0 A_0(\vec{y},y_0)C(0,0)\rangle}{\sum_{\vec{y}}\langle P(\vec{y},y_0)C(0,0)\rangle} \tag{2}$$

and this is also shown in Fig. 1.

As expected with a chiral action, no additive mass renormalization for the quark mass is observed. (The squared pion mass extracted from the correlator of two pseudoscalar cur-

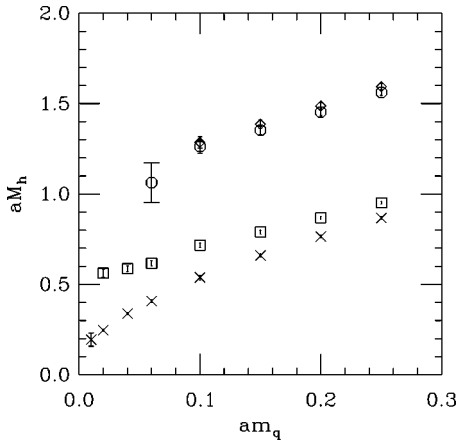

FIG. 2. Spectroscopy from the planar overlap action: crosses, pseudoscalar mesons; squares, vector mesons; octagons, nucleons; diamonds, deltas. The four lighter mass values are from the $12^3\times 24$ lattices.

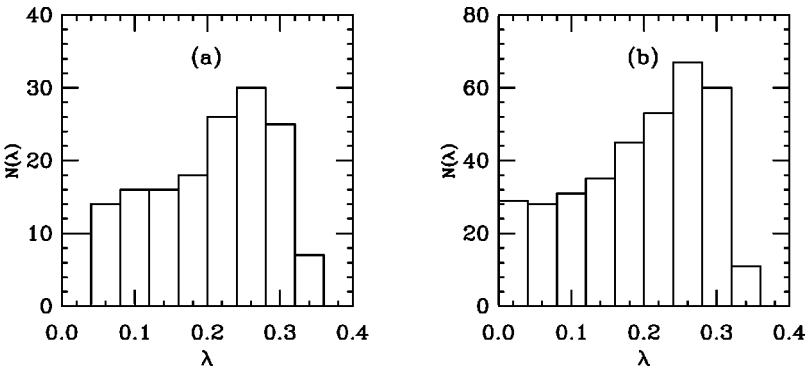

FIG. 3. Histograms of the number density of the imaginary part of the nonzero eigenmodes of the overlap Dirac operator. (a) Lowest 10 modes on 12^4 lattices; (b) lowest 20 modes on $12^3\times 24$ lattices.

rents does not extrapolate to zero linearly at small bare quark mass, though the mass extracted from the difference of the scalar correlator and the pseudoscalar correlator does. This might be a quenched approximation-finite volume artifact, as we discuss in Sec. IV.)

Results for spectroscopy are shown in Fig. 2. With the small data set, the noise in the baryon channels becomes too large for a stable mass fit at small quark mass. Making a naive extrapolation of the rho mass to the chiral limit and fixing the lattice spacing from the physical value of its mass would indicate a lattice spacing of about 0.13 fm, as opposed to a value of 0.11 fm from the Sommer parameter, using the interpolating formula of Ref. [24]. We will (somewhat arbitrarily) use the lattice spacing from the Sommer parameter to convert lattice numbers into dimensionful ones throughout the rest of the paper.

On the 12^4 lattices we calculated the ten lowest-eigenvalue eigenmodes of $D(0)$ on each configuration [more properly, we calculated the ten smallest eigenvalue modes of $H(0)^2$ in the chiral sector of the minimum eigenvalue, and reconstructed the degenerate eigenstate of opposite chirality when one was present]. On one configuration we found the lowest twenty eigenmodes. On the $12^3\times 24$ lattices we found the lowest twenty eigenmodes. Histograms of the number density of the imaginary part of the nonzero eigenmodes as a function of their value are shown in Fig. 3 for the two data sets. The smallest nonzero eigenmodes in both sets have a value of about 0.002 in lattice units, and the largest ones are about 0.3–0.35. With a nominal lattice spacing of 0.11 fm, this corresponds to eigenmodes in physical units ranging from 3.6 MeV to 640 MeV. To set the scale, a calculation of the chiral condensate with the same action in Ref. [20] gives $\langle\bar{\psi}\psi\rangle$ of roughly $(280\ \mathrm{MeV})^3$, and the lightest quark mass at which we have performed spectroscopy, $am_q=0.01$, corresponds to a quark mass of about 18 MeV.

We measured the topological charge density [which we denote as $Q(x)$] using an operator described in our previous work [25]. This operator is built of a sum of two perimeter-ten loops, twisted in four dimensions to provide a lattice approximation to $\mathrm{Tr}F_{\mu\nu}(x)\tilde{F}_{\mu\nu}(x)$. The links in the loops are built of APE-smeared links, and the operator can be tuned by the choice of α (0.45 in this study) and N (mostly set to 10). As a demonstration of the efficiency of the operator, we examined a set of smooth single instanton configurations, varying the radius ρ of the instanton. Our results are shown in Fig. 4. Without smearing the topological charge $Q=\int d^4xQ(x)$ decreases slowly from one to zero over a wide range of instanton radii as the instanton disappears from the lattice, while at large smearing levels it cuts off sharply. The fermion spectrum should (and does) possess a single, chiral zero mode for as long as the fermion couples to the instanton. When the instanton radius shrinks to some minimum value, the fermion cannot see the instanton and the zero mode disappears. This behavior is also plotted in Fig. 4. We see that the $\alpha=0.45$, $N=10$ gauge observable has a similar response to that of our fermion action [which is also built of (0.45,10) blocked links].

III. PROPERTIES OF LOW-LYING EIGENMODES

We begin by comparing the bulk quantities of our configurations. The Atiyah-Singer index theorem relates the topological charge and the number of exact fermionic zero modes of a configuration, $Q_{top}=n_+-n_-$. This relation does not hold exactly in our case as our definition of Q_{top} does not produce a value for the topological charge which is an integer, nor which is precisely the same as what the fermion observable experiences. Yet the number of zero modes and

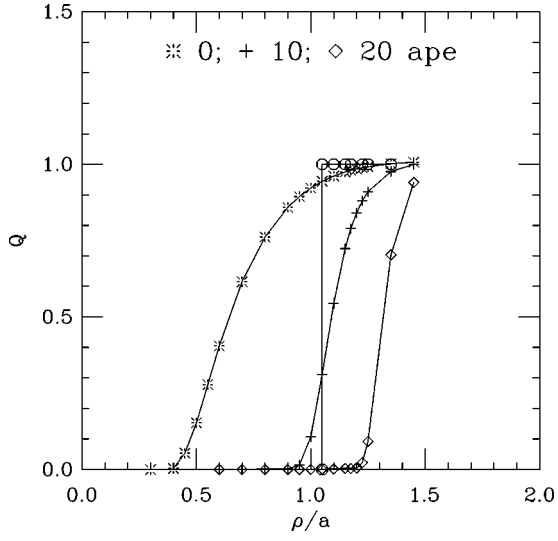

FIG. 4. Comparison of topological charge on a set of smooth single instanton configurations of varying instanton radius ρ. Octagons show the number of zero modes of the overlap fermion, while the other symbols show the topological charge measured by the pure gauge observable with various amounts of APE smearing.

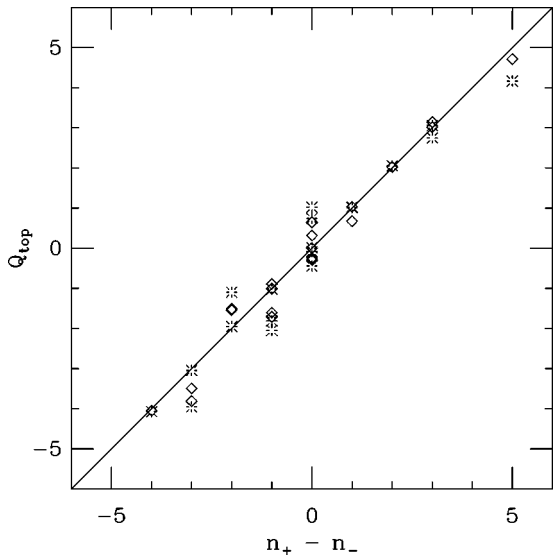

FIG. 5. Topological charge as measured by the pure gauge observable versus the number of fermion zero modes for our ensemble of configurations. Diamonds show 10 APE smearings for the gauge observable; bursts, 20 smearing steps.

the net topological charge are strongly correlated, as seen in Fig. 5.

An accurate measurement of the topological susceptibility $\chi=\langle Q^2\rangle/V$ requires large statistics. Nevertheless, the good agreement of the topological charge with the number of fermion zero modes justifies gauge measurements of χ. Nearly all groups [4] measure a value close to $\chi^{1/4}=180$–200 MeV. With our limited data set (on the 12^4 lattices) and taking the lattice spacing from the Sommer parameter we find $\chi^{1/4}=224\pm 17$ MeV using the fermionic zero modes to determine the topological charge. This error is purely statistical and includes no uncertainty due to the lattice spacing.

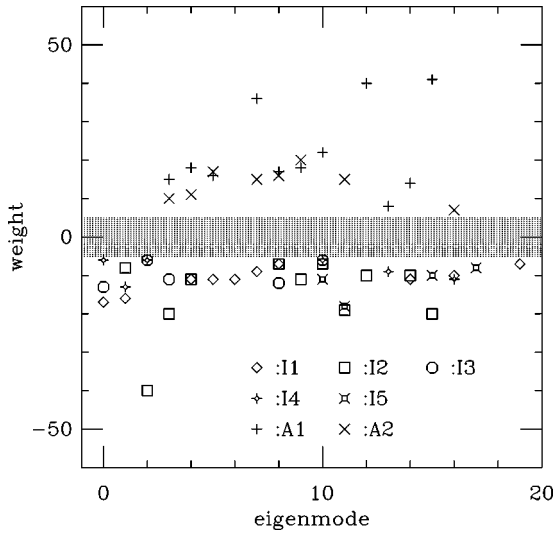

FIG. 6. The weight with which the most prominent 5 instantons and 2 anti-instantons couple to the first 20 eigenmodes of a typical 12^4 configuration. In the shaded region the background fluctuations are too strong to distinguish topological modes; therefore, that region in the graph is excluded. Observe that the first three modes (the chiral modes) couple only to the instantons, while the rest of the modes are distributed over both instantons and anti-instantons.

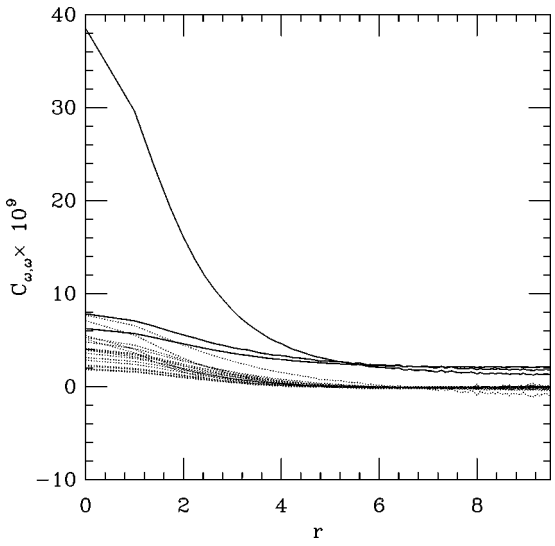

FIG. 7. Chirality correlation function for a 12^4 configuration with 3 zero modes (shown as solid lines), showing the additional 17 lowest non-chiral mode pairs (shown as dotted lines). The height of the correlator at the origin decreases more or less monotonically with the size of the eigenvalue of the mode.

Next, we examine the spatial distributions of the eigenmodes themselves. To do this, we compute the local chiral density $\omega(x)=\langle\psi(x)|\gamma_5|\psi(x)\rangle$ for each eigenmode $\psi(x)$ of the Dirac operator D. A glance at contour plots of this quantity reveals a rich structure of bumps. A pattern recognition program which recognizes the bumps reveals that the locations of maxima of different eigenmodes are strongly correlated, and that they are strongly correlated with the positions of maxima of $Q(x)$, the pure gauge observable. The (chiral)

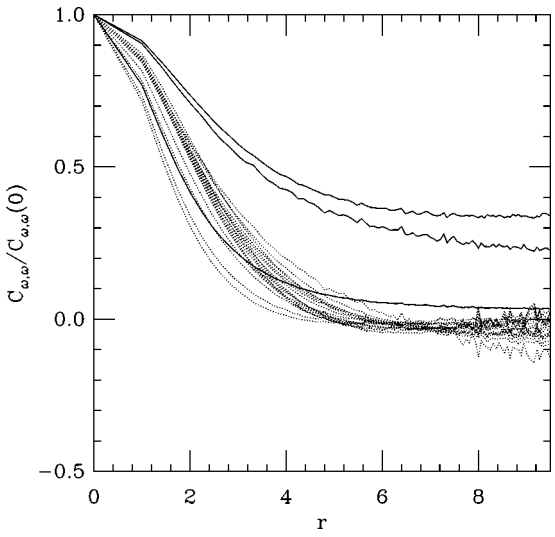

FIG. 8. The correlator of Fig. 7, scaled by the value of the correlator at the origin. Chiral modes are shown as solid lines, while the nonchiral modes are shown as dotted lines.

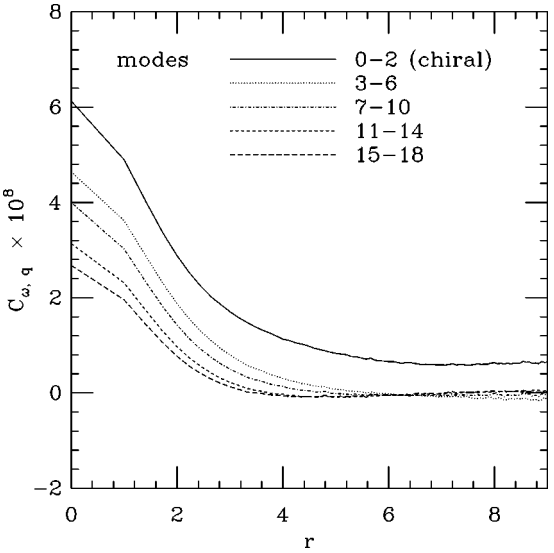

FIG. 9. Mixed topological charge-chirality correlation function for a typical configuration. The correlators for the three chiral modes are averaged, as are the correlators for groups of nonchiral modes (organized by increasing fermion eigenvalue).

zero modes are spread over maxima of $Q(x)$ that have the opposite sign [$\omega(x)$ is negative on instantons where $Q(x)$ is positive]. The volume integral of $\omega(x)$ is zero for the nonchiral modes. These modes have both positive and negative peaks. The locations of these peaks correlate with the appropriate sign peaks of $Q(x)$. As long as the individual peaks are well separated we can fit the chiral density in terms of single instanton modes

$$\omega(x)=\sum_i c_i \omega_\rho^0(x-x_i)+\eta(x), \tag{3}$$

where $\omega_\rho^0(x)$ is the (classical) chiral density of a single instanton of radius ρ and location $x=0$, and $\eta(x)$ represents

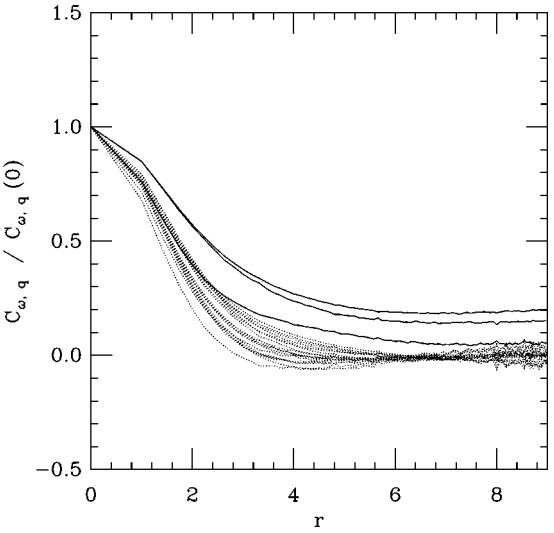

FIG. 10. Mixed topological charge-chirality correlation function for the configuration of Fig. 9, scaled to its value at the origin. Chiral modes are solid; nonchiral ones, dotted.

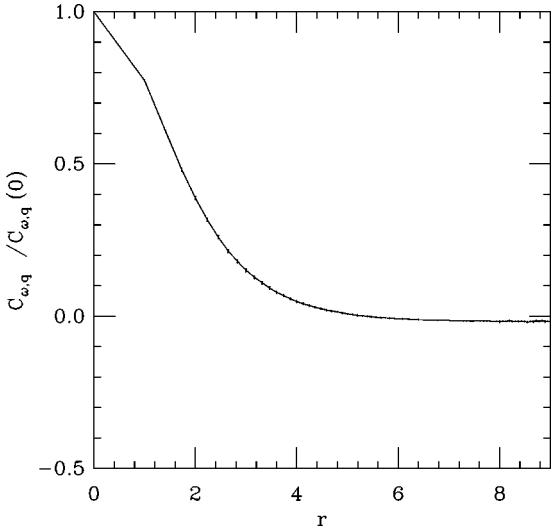

FIG. 11. Mixed topological charge-chirality correlation function averaged over all the nonchiral modes on all 12^4 configurations in the data set.

the part of the chiral density not associated with well separated instantons. The coefficients $c_i>0$ for anti-instantons and $c_i<0$ for instantons.

We consider one 12^4 configuration in detail. This configuration has topological charge $Q=3$ according to both the gauge observables and the fermionic definition. After 10 APE steps the instanton pattern recognition code identifies 7 instantons and 5 anti-instantons on the gauge configuration. After an additional 10 APE steps the gauge configuration is considerably smoother, and we can identify only 4 of the instantons and 2 of the anti-instantons, although the integrated topological charge is still 3. Obviously the pattern recognition algorithm misinterprets some object(s).

The chiral density function $\omega(x)$ peaks at the same locations as $Q(x)$. It couples strongly to all the objects found

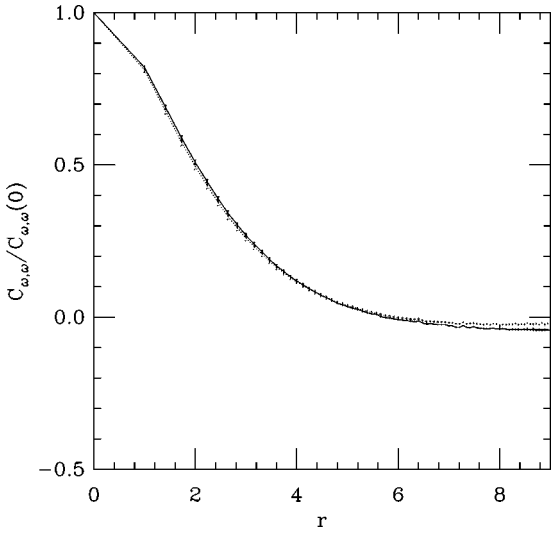

FIG. 12. Chirality autocorrelation function averaged over all the nonchiral modes on all configurations in the data set. The lower curve corresponds to 12^4 lattices; the upper one to $12^3\times 24$ lattices.

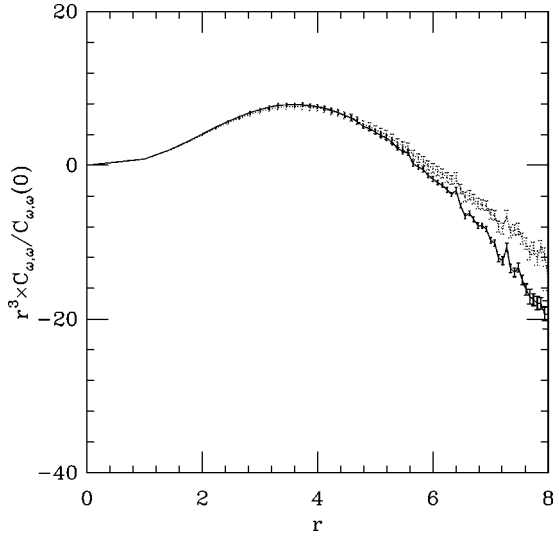

FIG. 13. The same data as Fig. 12, but scaled by r^3 to expose the large distance tail. The solid curve corresponds to 12^4 lattices; the dotted one to $12^3 \times 24$ lattices.

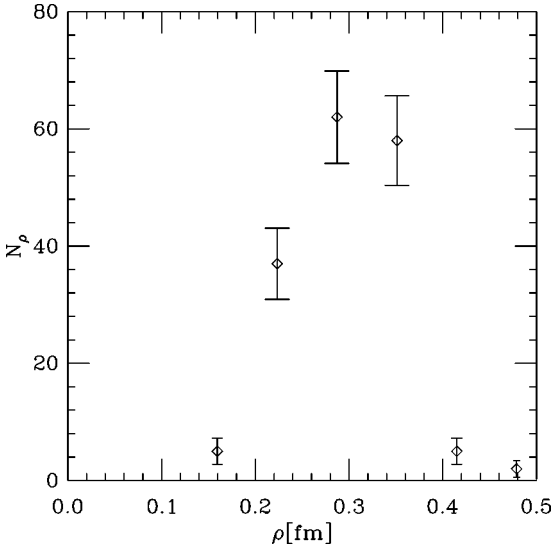

FIG. 14. Instanton number density vs size, extracted from the fermion chirality density function, and converted to physical units using a nominal lattice spacing of $a=0.11$ fm.

after 20 APE steps, 4 instantons and 2 anti-instantons, and picks up a fifth instanton found after 10 but not 20 smoothing steps. With smaller weights it peaks at other locations as well, possibly identifying nearby pairs. The different eigenmodes couple to the different topological objects with varying weights. In Fig. 6 we show the weight relative to the background fluctuations,

$$w_i = \frac{c_i}{\sqrt{\langle \eta^2 \rangle}}, \tag{4}$$

with which the most prominent 5 instantons and 2 anti-instantons couple to the first 20 eigenmodes. $\sqrt{\langle \eta^2 \rangle}$ is the average of the local chiral density $\omega(x)^2$ for space-time points that are not associated with any topological objects [see Eq. (3)]. In order to identify a mode we require that its weight is at least five times above background, $w_i > 5$; therefore the shaded region in the graph is excluded. Observe from the figure that the first three modes (the chiral modes) couple only to the instantons, while the rest of the modes are

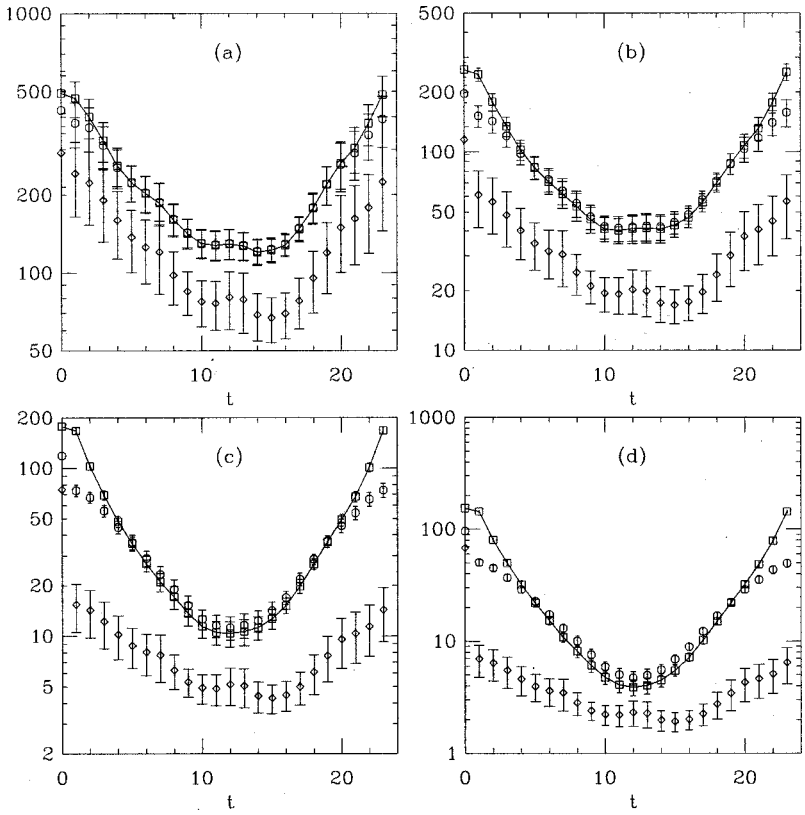

FIG. 15. Saturation of the pseudoscalar correlator by low-lying eigenmodes of $H(0)^2$. (a) $am_q=0.01$ ($\pi/\rho \simeq 0.34$); (b) $am_q=0.02$ ($\pi/\rho \simeq 0.50$); (c) $am_q=0.04$ ($\pi/\rho \simeq 0.61$); (d) $am_q=0.06$ ($\pi/\rho \simeq 0.64$). Squares (connected by lines) show the full hadron correlator. Octagons show the contribution from the lowest 20 modes. Diamonds show the contribution from the zero modes.

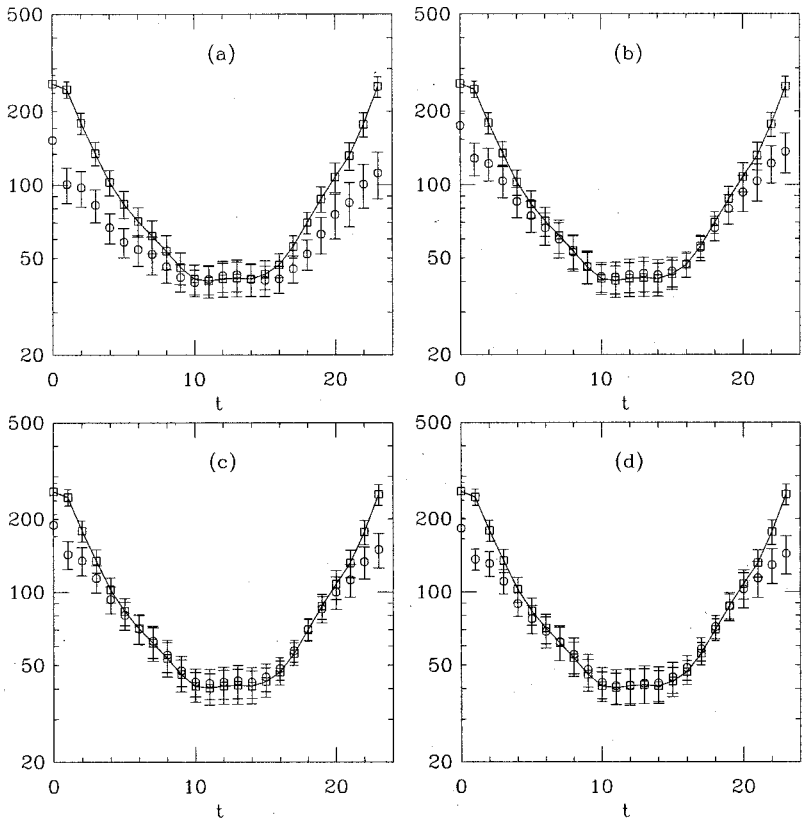

FIG. 16. Saturation of the pseudoscalar correlator by low-lying eigenmodes of $H(0)^2$ at $am_q=0.02$ $(\pi/\rho\simeq 0.50)$. Squares (connected by lines) show the full hadron correlator. Octagons show the contributions from the lowest N modes, where in (a) $N=4$, in (b) $N=8$, in (c) $N=12$, in (d) $N=16$.

distributed over both instantons and anti-instantons. Most modes couple with weights 10–20 to several topological objects, but occasionally the mode overwhelmingly couples to a single topological object. For example the third chiral mode couples very strongly to one of the instantons, I2. I2 is the smallest topological object identified on the configuration, with a radius $\rho/a\simeq 2.0$, but it is not obvious to us that that explains the unusually large coupling.

There is no qualitative difference between the lowest and highest non-chiral modes: they couple to the same set of topological objects with slightly decreasing magnitude. The volume of this configuration is about 4 fm^4, so according to the instanton-liquid model one would expect around 4 well defined objects. Indeed the pattern recognition code identifies about half a dozen topological objects, yet every one of the lowest 20 eigenmodes shows strong coupling to them and there is no reason to believe that the situation will change if we consider the next 10 or 20 eigenmodes. They all couple to the same set of topological modes in addition to non-topological, ''spin-wave'' modes. As the eigenvalue increases, the coupling to the topological modes decreases while the spin wave mode coupling increases, until it is no longer possible to actually separate the topological modes from the background. The $12^3\times 24$ configurations show a similar pattern but with more topological objects, as is expected in a larger volume.

To further quantify these observations, we construct the autocorrelation function of chirality

$$C_{\omega,\omega}(r)=\frac{1}{V}\int d^3x\,\omega(x)\omega(r+x) \tag{5}$$

and the correlation function of chirality with topological charge

$$C_{\omega,Q}(r)=\frac{1}{V}\int d^3x\,\omega(x)Q(r+x). \tag{6}$$

Let us first consider $C_{\omega,\omega}(r)$ on the same $Q=3$ configuration as above, shown in Fig. 7. We show the autocorrelator for each of the lowest 20 modes, chiral and nonchiral. The peak at small r indicates that the chirality is localized. The three solid lines correspond to the three chiral zero modes. The very large autocorrelator corresponds to the third chiral mode, which has an unusually large coupling to one of the instantons, I2 in Fig. 6. The amount of localization of a mode dies away slowly as the eigenvalue of the mode increases. [The autocorrelation function of the zero modes does not fall to zero because $\omega(x)$ integrates to unity, while $\int\omega(x)=0$ for the nonchiral modes.] However, the size of the localized region does not depend too much on the magnitude of the eigenvalue. We can see that by normalizing the autocorrelator by its value at the origin, in Fig. 8.

Similar features are seen for the mixed correlator. Where the topological charge is large, there also $\omega(x)$ peaks. Higher modes gradually decorrelate with topological charge. Nevertheless, the size of the correlated region depends only weakly on the eigenvalue. Compare Figs. 9 and 10.

Now we combine all the lattices in our data set and average our correlation functions over all the nonchiral modes. The correlation function for the chirality with the topological charge and the autocorrelation function of the chirality are shown in Figs. 11 and 12. (There really are error bars in

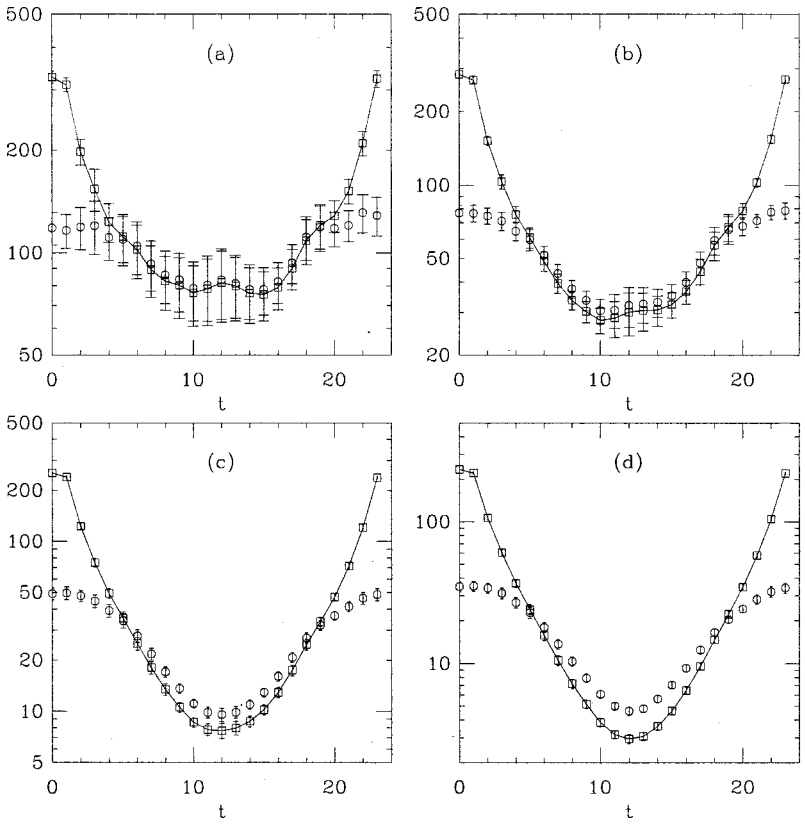

FIG. 17. Saturation of the difference of pseudoscalar and scalar correlators by the 20 low-lying eigenmodes of $H(0)^2$. Squares (connected by lines) show the full hadron correlator. Octagons show the contribution from the lowest 20 modes. (a) $am_q=0.01$ ($\pi/\rho\simeq 0.34$); (b) $am_q=0.02$ ($\pi/\rho\simeq 0.50$); (c) $am_q=0.04$ ($\pi/\rho\simeq 0.61$); (d) $am_q=0.06$ ($\pi/\rho\simeq 0.64$).

these pictures.) The chirality autocorrelation function is slightly broader than the mixed correlator, which is not surprising as the fermionic zero mode wave function falls off more slowly than the topological charge density. Figure 12 actually has two curves: one corresponds to the 12^4, the other to the $12^3\times 24$ data set. The two curves are almost indistinguishable except at large distances where, due to the periodicity of the lattice, the 12^4 curve falls somewhat below the other. From the falloff of the correlator one can estimate the typical size of the instantons to be about three lattice spacings or 0.3 fm. The fermionic wave functions are slightly larger than that. One would expect to see finite size effects when the lattice size is comparable to the diameter of the wave function, about 1 fm.

All of these features are exactly what one would expect based on the instanton liquid model of the QCD vacuum [2]: The (degenerate) chiral modes are on the appropriate charge instantons, coupling to all of them. The nonchiral modes are made of a superposition of peaks, each peak centered on an instanton or an anti-instanton, and interpolating among them.

If the chirality correlator was ''lumped,'' and interpolated between opposite sign peaks on instantons and anti-instantons, one would also expect that $C_{\omega,\omega}(r)$ would go negative at large r, as an instanton peak (one sign of chirality) would anti-correlate with a nearby anti-instanton peak (opposite chirality). Figure 13 multiplies the autocorrelator by the phase space factor of r^3 and exposes this behavior. Similar negative correlation was observed using the pure gauge topological charge operator in Ref. [26].

Finally, we can determine a size distribution of the topological objects seen by the fermions. We do this by identifying peaks in the distribution of $\omega(x)$, and fitting the peak shape to the shape expected from a fermionic zero mode. The radius of the peak is directly related to the instanton radius ρ. This is basically the same procedure that is used to identify instantons with the pure gauge local charge distribution $Q(x)$. It suffers from the same limitations—a bump must stand out from the background high enough to be seen, and must not die away too quickly. The first constraint means that large objects will be lost (large ρ instantons have a flat profile); the second constraint means that small instantons will also not be seen. The resulting distribution is shown in Fig. 14, where we have converted our result to physical units using a nominal lattice spacing of $a=0.11$ fm. The distribution peaks around $\rho=0.3$ fm. This value is quite similar to that from a pure gauge calculation by one of us [25], considerably smaller than that of two other pure gauge calculations [27,28], and quite consistent with the expectations of instanton liquid phenomenology [2,29].

IV. WHAT DO THESE EIGENMODES DO?

In the last section we demonstrated that the low lying eigenmodes of the Dirac operator are strongly correlated with the topological structure in the QCD vacuum. But are these modes relevant to any physical processes? Phenomenological instanton models predict that light quarks propagate in the vacuum by hopping between oppositely charged topological objects, and therefore the lightest hadron propagators are dominated by the low lying fermion modes. There are three obvious classes of observables to investigate: ordinary hadronic correlators, point-to-point correlators, and discon-

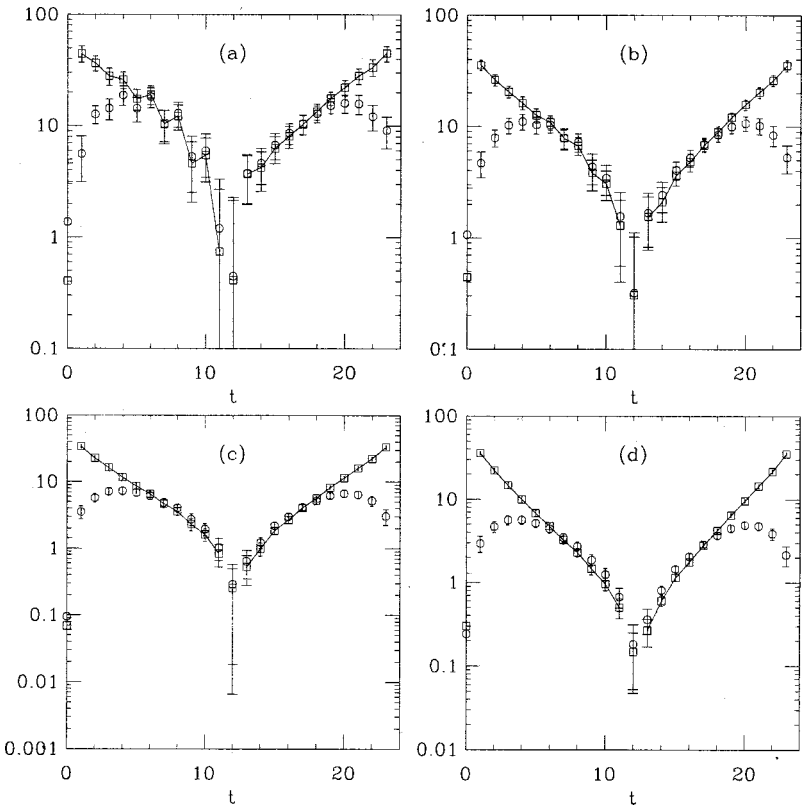

FIG. 18. Comparison of the correlators needed to compute the PCAC quark mass and f_π: the (absolute value of the) pseudoscalar source—axial vector sink correlators of the numerator of Eq. (2). Squares (connected by lines) show the full hadron correlator. Octagons show the contribution from the lowest 20 modes. (a) $am_q=0.01$ ($\pi/\rho\simeq 0.34$); (b) $am_q=0.02$ ($\pi/\rho \simeq 0.50$); (c) $am_q=0.04$ ($\pi/\rho\simeq 0.61$); (d) $am_q = 0.06$ ($\pi/\rho\simeq 0.64$).

nected (hairpin) diagrams. We have chosen to focus on the first class, since they directly probe the behavior of QCD at large distances and are relevant to most measurements of hadronic matrix elements. (The latter observables are obviously targets for future study.)

We constructed sets of quark propagators on the $12^3 \times 24$ data set at several values of the quark mass via a usual calculation, and built complementary sets of propagators in which the quark propagator was approximated by a mode sum over the lowest N (2 to 20) modes. In both cases we used a Coulomb-gauge Gaussian source and projected the point sink of the correlator onto zero momentum. We will compare the correlators at lattice quark mass $am_q=0.01$, 0.02, 0.04, and 0.06, corresponding to a pseudoscalar/vector meson mass ratio of about 0.34, 0.50, 0.61 and 0.64.

Approximating the quark propagator by a truncated mode sum is obviously uncontrolled, and we would not advocate doing it in a real calculation. However, it serves as a naive realization of an instanton liquid model.

First, we must make a digression to discuss the effect of the exact zero modes. There are hadron correlators which are sensitive to zero modes and ones which are not [30]. Since the zero modes are chiral, the zero mode quark propagator is proportional to $(1\pm\gamma_5)$ and inversely proportional to $1/m_q$. Because of its Dirac structure it couples to the pseudoscalar-pseudoscalar (Ps-Ps) and scalar-scalar (S-S) correlators. At small quark mass it makes an ever larger contribution to these correlators, dominating them in the chiral limit in finite volumes. This contribution is a quenched approximation finite-volume lattice artifact: quenched, because the zero mass limit of full QCD has no zero modes, and a finite-volume effect because the number of zero modes compared to the number of nonchiral modes is volume-dependent. For example, in the Gell-Mann–Oakes-Renner (GMOR) relation, the volume-averaged point-to-point Ps-Ps correlator $\Sigma_x\langle\pi(x)\pi(0)\rangle/V$ has a contribution $Q/(m_q^2V)$ in addition to a volume-independent piece from the nonchiral modes. This piece actually scales like $1/\sqrt{V}$ because $\langle Q^2\rangle\simeq V$. The axial current autocorrelator can have ''mixed'' contributions (one quark propagating through a zero mode and the other quark through nonzero modes), and the zero modes can be completely decoupled from the pseudoscalar channel by considering the difference of a Ps-Ps and S-S correlator.

TABLE I. PCAC quark mass and pseudoscalar decay constant from full propagators and from 20-mode truncations.

am_q	Full m_q	20-mode m_q	Full af_π	20 mode f_π
0.01	0.009(1)	0.011(2)	0.092(8)	0.100(12)
0.02	0.020(1)	0.017(2)	0.091(4)	0.100(6)
0.04	0.041(1)	0.032(2)	0.092(2)	0.085(5)
0.06	0.062(1)	0.046(2)	0.093(2)	0.085(10)

Since the overall $1/m_q$ coefficient allows the zero modes to dominate some correlators, a conventional extraction of masses from exponential decay when m_q is much smaller than the eigenvalue of the first nonzero mode would give a prospective pion mass that is independent of the quark mass (because it is related to the correlations inherent in the zero modes). We believe that this artifact might be related to the flattening of the pion mass seen in the Ps-Ps correlator at $am_q=0.04$ and 0.06 in Fig. 1. From this correlator, the low-

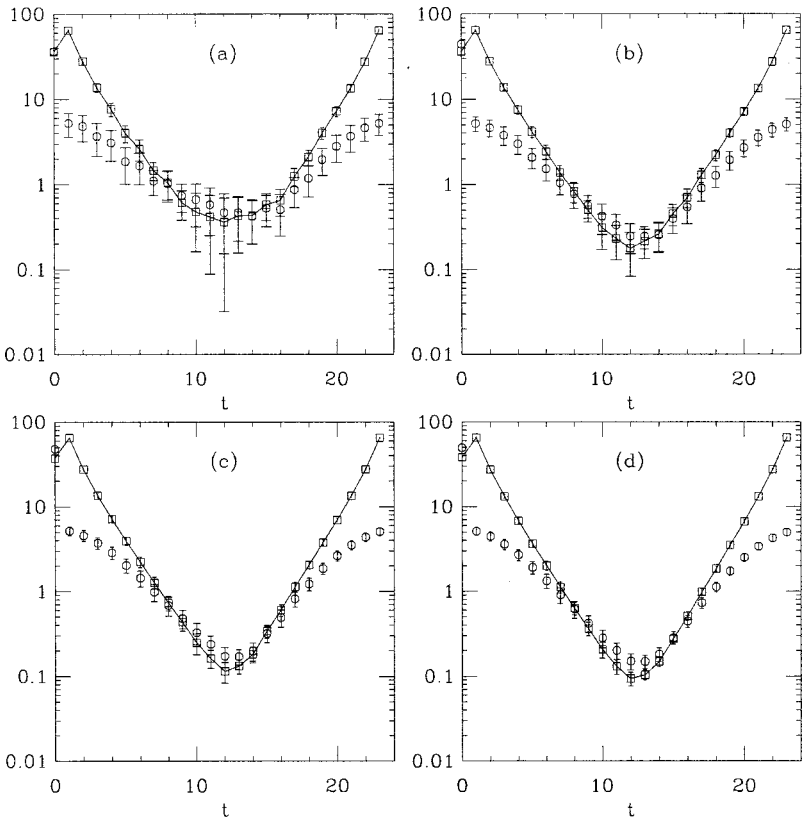

FIG. 19. Comparison of the full vector meson correlator (squares) with the correlator built from the lowest 20 eigenmodes of $H(0)^2$ (octagons). (a) $am_q=0.01$ ($\pi/\rho\simeq 0.34$); (b) $am_q=0.02$ ($\pi/\rho\simeq 0.50$); (c) $am_q=0.04$ ($\pi/\rho\simeq 0.61$); (d) $am_q=0.06$ ($\pi/\rho\simeq 0.64$).

est four points give a lattice squared pion mass of $(am_\pi)^2=0.018(4)$ at zero bare quark mass. The pion mass extrapolated from the difference between Ps-Ps and S-S correlators, shown in the figure as octagons, extrapolates to $(am_\pi)^2=0.008(5)$ at zero quark mass.

The vector current, $\gamma_i\gamma_5$ axial current, and the nucleon and delta all have no coupling to the zero modes.

We find from our data that at small quark mass the low modes saturate the hadron correlators at large time separations. As more modes are added, the saturation extends to lower and lower times. This effect decreases as the quark mass rises.

A. Pseudoscalar and scalar correlators

The most dramatic effects are seen in the pseudoscalar and scalar channels. At our lowest mass (pseudoscalar/vector meson mass ratio of about 0.34) the saturation seems complete, and at higher masses it is less so. In Fig. 15 we compare the full propagator and the $N=20$ truncated propagator for the pseudoscalar channel. Twenty eigenmodes saturate the propagator even at our heaviest quark mass, $am_q=0.06$. While the chiral modes themselves do not saturate the propagator (also shown in Fig. 15), at low mass, only a few modes are needed. Results on varying the number of modes used to saturate the pseudoscalar correlator at $am_q=0.02$ are shown in Fig. 16. At $am_q=0.02$ 8–12 modes saturate the propagator. This is in agreement with instanton models that suggest that the number of relevant modes is about the same as the number of instantons on the lattice. With an instanton density of one per fm^4 on our $12^3\times 24\approx 8$ fm^4 lattices we indeed expect about 8 instantons per lattice. Results for the other quark masses are similar though the number of modes needed to saturate the propagator rises to about 12–16 modes at $\pi/\rho\simeq 0.64$. Saturation of the pseudoscalar-scalar differ-

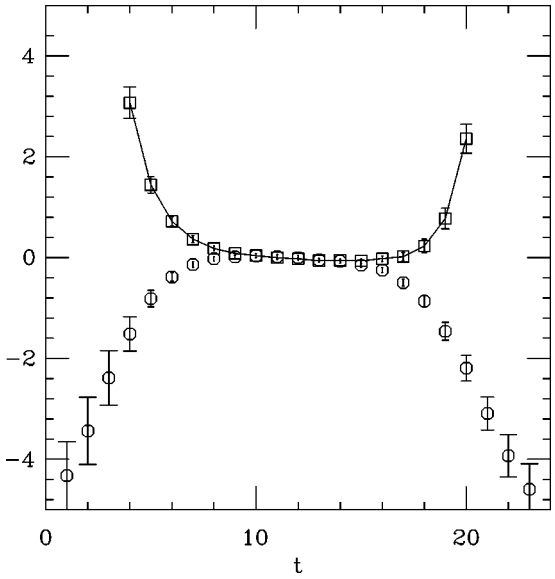

FIG. 20. Comparison of the full axial vector meson correlator with the correlator built from the lowest twenty eigenmodes of $H(0)^2$, at bare quark mass 0.04. Squares are the full correlator; octagons, 20-eigenmode truncation.

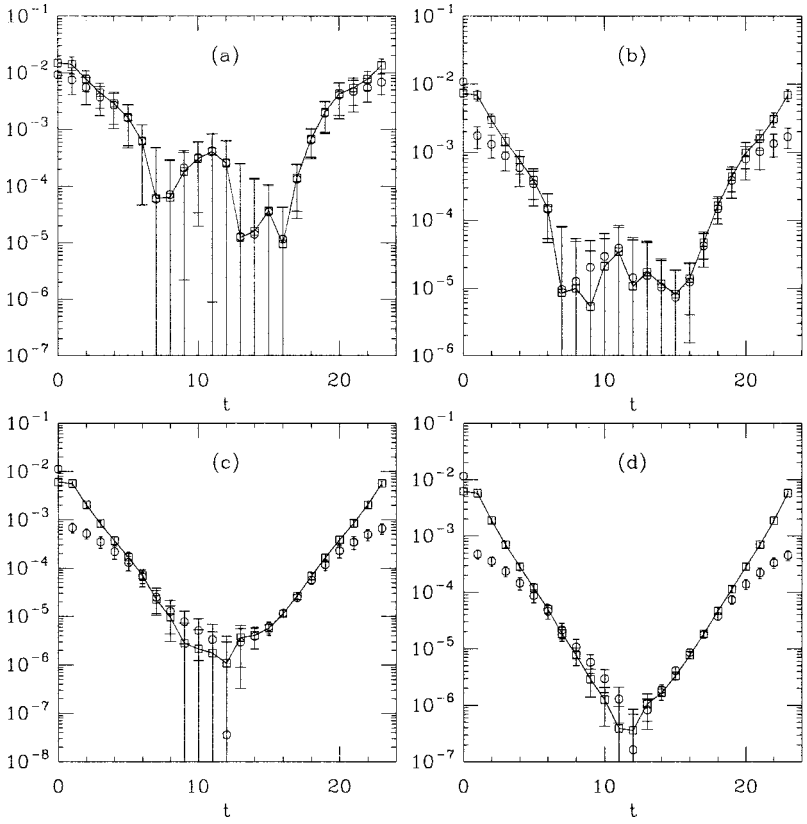

FIG. 21. Comparison of the full nucleon correlator (squares) with the correlator built from the lowest 20 eigenmodes of $H(0)^2$ (octagons). (a) $am_q=0.01$ $(\pi/\rho\simeq 0.34)$; (b) $am_q=0.02$ $(\pi/\rho \simeq 0.50)$; (c) $am_q=0.04$ $(\pi/\rho\simeq 0.61)$; (d) $am_q =0.06$ $(\pi/\rho\simeq 0.64)$.

ence correlator (to which zero modes do not contribute) is shown in Fig. 17.

To orient the reader, keeping the lowest ten eigenmodes amounts to keeping only eigenmodes of the Dirac operator whose imaginary part is less than about 350 MeV.

We also looked at the simplest quantities related to chiral symmetry that we can extract from our data, the PCAC quark mass and the pseudoscalar decay constant. The same numerator is used in the lattice measurement of the PCAC quark mass [Eq. (2)] and the pseudoscalar decay constant $f_{PS}\simeq\langle\pi|A_0|0\rangle$. Overlap fermions satisfy the GMOR relation mode by mode. This is not the case for the PCAC relation, although one would expect that a chiral theory would also respect it. What do low eigenmode truncations give for these quantities?

The numerators of the relevant correlators are shown in Fig. 18. The source $C(0,0)$ is a Gaussian source (γ_5). This picture plus Fig. 15 serve to show that the average pseudoscalar correlator is reproduced using only the lowest fermion modes in the quark propagator, even at short t. By longer t, the axial current matrix element is also saturated by the low lying modes. Thus both the PCAC quark mass and f_π will be correctly computed using these truncated propagators at small quark mass—as a straightforward fit shows (see Table I). Note that by $am_q=0.06$ the 20-mode PCAC quark mass deviates from the full calculation. This quark mass is about one fifth of the value of the largest eigenmode kept in the mode sum.

B. Vector and axial vector correlators

We observe that the vector meson correlator saturates only at a much larger time separation than the pseudoscalar correlator. This is not very surprising based on instanton model phenomenology [2]. The two quarks of the vector meson have to couple to two different instantons to propagate chirally. That requires a propagation distance about twice the instanton size; at shorter distances the quarks of the vector meson propagate like free particles, independent of the instanton modes of the Dirac operator. This is shown in Fig. 19.

The signal in the axial vector channel is much noisier, and if the mode sum and the full propagators resemble each other, it is only after our signal has disappeared into the noise. At low t the low mode correlator even has the opposite sign to the full correlator. Compare Fig. 20.

C. Baryon correlators

Both baryon signals (proton and delta) become increasingly noisy at small quark mass. However, it appears that the low-lying fermionic modes do a better job of saturating the nucleon correlator than the delta correlator. Compare Figs. 21 and 22.

These features are in complete agreement with simple instanton-based phenomenology [2]: In the instanton liquid, different flavor quarks can travel together from instanton to instanton, exchanging their flavor and flipping their spin. In pseudoscalar and scalar meson channels, the quantum numbers of the quarks allow this kind of propagation. Nucleons contain a spin-zero ud diquark which can also propagate in this way. The lower the value of the eigenmode, the more it couples to instantons, and so the low eigenmodes dominate the correlator. Vector mesons, however, lack first order instanton interactions but do interact in second order. The di-

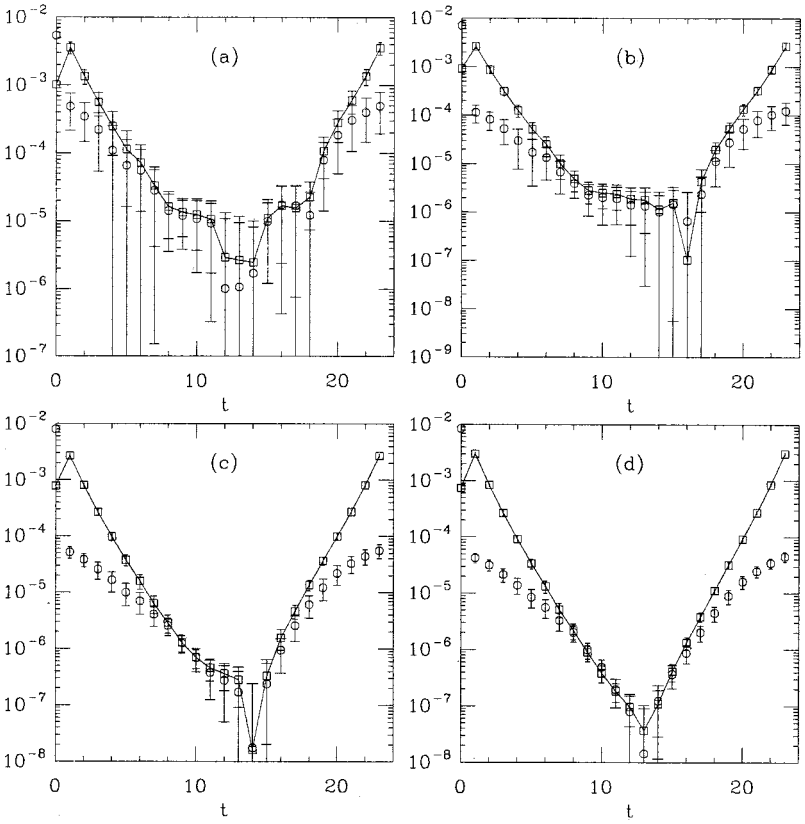

FIG. 22. Comparison of the full delta correlator (squares) with the correlator built from the lowest 20 eigenmodes of $H(0)^2$ (octagons). (a) $am_q=0.01$ $(\pi/\rho\simeq 0.34)$; (b) $am_q=0.02$ $(\pi/\rho\simeq 0.50)$; (c) $am_q=0.04$ $(\pi/\rho\simeq 0.61)$; (d) $am_q=0.06$ $(\pi/\rho\simeq 0.64)$.

quarks in the delta are all in $j=1$ states and cannot experience first-order interactions either.

According to the calculations in Refs. [31] and [2], the important parameter of the instanton liquid phenomenology is the tunneling amplitude between instantons and anti-instantons,

$$\langle |T_{IA}|^2\rangle = \frac{2\pi^2}{3N_c}\frac{N}{V}\rho^2, \tag{7}$$

and with a mean instanton size of $\rho\simeq 1/3$ fm and density $N/V\simeq 1$ fm^{-4}, $|T_{IA}|\simeq 90$ MeV. The quark propagator for quark mass m in the zero-mode zone has a denominator of roughly $T+im$ and one might expect that, when m becomes comparable to T_{IA}, replacing the full propagator by a sum over instantons might be a bad approximation. A lattice regulated bare quark mass of about 100 MeV would correspond roughly to $ma\simeq 0.06$, which is actually the place where we observe that the lowest modes (whose values are less than 640 MeV) begin not to saturate any correlator.

Our remarks apply only to long distance correlation functions, not to short distance point-to-point correlators, nor to vacuum-to-vacuum diagrams (hairpins), neither of which we have yet investigated. Point-to-point correlators look at QCD at short to intermediate distances and the results from these simulations cannot be compared directly with ours. None the less, Ivanenko and Negele [32] have tried to saturate the pseudoscalar and vector point to point correlators with low lying eigenmodes. With 128 modes both correlators can be saturated.

Venkataraman and Kilcup [33] studied long distance correlators on dynamical lattices. They found that the pion correlator (at a pseudoscalar/vector meson mass ratio of 0.55, from the data set of Ref. [34]) could not be saturated by the 32 lowest modes. Their lattice volume is somewhat larger than ours, and their action is less chiral which can explain why their findings are different.

Several groups [33,35] have reported that pseudoscalar hairpins are saturated by low eigenmodes.

Finally, we [36] and Kovacs [37] have tried to study the effects of instantons in chiral symmetry breaking by isolating the instantons in a gauge configuration and reconstructing a pure multi-instanton configuration. Ordinary hadron spectroscopy using some standard (nonchiral) action is then computed on these configurations. The vector channel (especially as seen by Ref. [37]) is dominated by a very low mass excitation even at higher quark masses. These results qualitatively resemble the picture of the low mode correlators of Figs. 15 and 19.

V. CONCLUSIONS

Instantons seem to be responsible for most chiral symmetry breaking in quenched QCD on the lattice, with a lattice spacing near 0.11 fm. The lowest-eigenvalue eigenmodes of the Dirac operator have structure that is strongly correlated with the locations of instantons and anti-instantons. Low-lying nonchiral modes make a large contribution to light quark mass hadron propagators in channels where instanton liquid phenomenology would predict they would. Our little instanton liquid calculation indicates that the instanton pic-

ture should break down at larger quark masses, as we observe.

Of course, there is no reason for instantons to be the whole story. While on even smoother lattices one expects that instantons will be equally important, in the strong coupling limit chiral symmetry is broken in QCD without any recourse to instantons [38]. Some vestige of this mechanism of chiral symmetry breaking might persist to the continuum limit. Also, Fig. 14 shows that the mean instanton size seen by our fermions is about 0.3 fm. A larger lattice spacing will compromise these objects. One might expect a different physical picture of chiral symmetry breaking in lattice simulations in that case.

Note also that instantons cannot account for the behavior of the pion at larger quark mass. From Fig. 1 we see that the linear relation between the squared pion mass and the quark mass persists to well above a pseudoscalar/vector mass ratio of 0.8, where the light modes we have identified no longer saturate the pion correlator. One would still say that the pion exhibits pseudo-Goldstone boson behavior in spite of the fact that the low lying modes become progressively less important. One might imagine that more modes might saturate the correlator. However, the qualitative features of instanton liquid phenomenology are supposed to involve only about as many modes as there are instantons, so the need for more than a few modes in our simulation volume begins to conflict with this phenomenology.

Nevertheless, in the real world, the up and down quarks are light. Our work suggests strongly that instantons affect their dynamics.

ACKNOWLEDGMENTS

Conversations with I. Horvath and H. Thacker inspired this work. Conversations with J. Negele and E. Shuryak sharpened our arguments. We are deeply grateful for the design and construction of our Beowulf cluster by Doug Johnson. This work was supported by the U.S. Department of Energy.

[1] T. Banks and A. Casher, Nucl. Phys. **B169**, 103 (1980).
[2] T. Schafer and E. V. Shuryak, Rev. Mod. Phys. **70**, 323 (1998).
[3] Cf. D. Diakanov, lectures given at the Enrico Fermi School in Physics, Varenna, 1995, hep-ph/9602375.
[4] J. W. Negele, Nucl. Phys. B (Proc. Suppl.) **73**, 92 (1999).
[5] See P. Hasenfratz and F. Niedermayer, Nucl. Phys. **B414**, 785 (1994); P. Hasenfratz, *ibid.* **B525**, 401 (1998); hep-lat/9803027, and references therein.
[6] M. Blatter, R. Burkhalter, P. Hasenfratz, and F. Niedermayer, Phys. Rev. D **53**, 923 (1996).
[7] See, for example, J. Smit and J. C. Vink, Nucl. Phys. **B286**, 485 (1987); **B298**, 557 (1988); Phys. Lett. B **194**, 433 (1987).
[8] For (a very incomplete listing of) examples of studies of topology with non-chiral fermion actions, see R. G. Edwards, U. M. Heller, R. Narayanan, and R. L. Singleton, Nucl. Phys. **B518**, 319 (1998); R. G. Edwards, U. M. Heller, and R. Narayanan, Phys. Rev. D **60**, 034502 (1999); T. DeGrand, A. Hasenfratz, and T. G. Kovacs, Nucl. Phys. **B547**, 259 (1999); P. H. Damgaard, U. M. Heller, R. Niclasen, and K. Rummukainen, *ibid.* **B583**, 347 (2000).
[9] For complementary reviews, see F. Niedermayer, Nucl. Phys. B (Proc. Suppl.) **73**, 105 (1999); H. Neuberger, *ibid.* **83-84**, 67 (2000).
[10] H. Neuberger, Phys. Lett. B **417**, 141 (1998); Phys. Rev. Lett. **81**, 4060 (1998).
[11] P. H. Ginsparg and K. G. Wilson, Phys. Rev. D **25**, 2649 (1982).
[12] R. G. Edwards, U. M. Heller, and R. Narayanan, Nucl. Phys. **B540**, 457 (1999).
[13] P. Hernandez, K. Jansen, and M. Lüscher, Nucl. Phys. **B552**, 363 (1999).
[14] A. Borici, Phys. Lett. B **453**, 46 (1999).
[15] R. G. Edwards, U. M. Heller, J. Kiskis, and R. Narayanan, Phys. Rev. D **61**, 074504 (2000).
[16] R. G. Edwards, U. M. Heller, and R. Narayanan, Parallel Comput. **25**, 1395 (1999).
[17] R. G. Edwards, U. M. Heller, J. Kiskis, and R. Narayanan, Phys. Rev. Lett. **82**, 4188 (1999).
[18] P. Hernandez, K. Jansen, and L. Lellouch, Phys. Lett. B **469**, 198 (1999).
[19] S. J. Dong, F. X. Lee, K. F. Liu, and J. B. Zhang, Phys. Rev. Lett. **85**, 5051 (2000); K. F. Liu *et al.*, Nucl. Phys. B (Proc. Suppl.) **94**, 752 (2001).
[20] MILC Collaboration, T. DeGrand, Phys. Rev. D **63**, 034503 (2001).
[21] APE Collaboration, M. Albanese *et al.*, Phys. Lett. B **192**, 163 (1987); M. Falcioni, M. L. Paciello, G. Parisi, and B. Taglienti, Nucl. Phys. **B251**, 624 (1985).
[22] See B. Bunk, K. Jansen, M. Lüscher, and H. Simma, DESY report, 1994; T. Kalkreuter and H. Simma, Comput. Phys. Commun. **93**, 33 (1996).
[23] Compare B. Jegerlehner, Nucl. Phys. B (Proc. Suppl.) **63**, 958 (1998); hep-lat/9612014; A. Frommer, B. Nockel, S. Gusken, T. Lippert, and K. Schilling, Int. J. Mod. Phys. C **6**, 627 (1995).
[24] ALPHA Collaboration, M. Guagnelli, R. Sommer, and H. Wittig, Nucl. Phys. **B535**, 389 (1998).
[25] T. DeGrand, A. Hasenfratz, and T. G. Kovacs, Nucl. Phys. **B505**, 417 (1997); **B520**, 301 (1998); A. Hasenfratz and C. Nieter, Phys. Lett. B **439**, 366 (1998).
[26] A. Hasenfratz, Phys. Lett. B **476**, 188 (2000).
[27] P. de Forcrand, M. Garcia Perez, J. E. Hetrick, and I. Stamatescu, hep-lat/9802017; Nucl. Phys. B (Proc. Suppl.) **63**, 549 (1998).
[28] UKQCD Collaboration, D. A. Smith and M. J. Teper, Phys. Rev. D **58**, 014505 (1998).
[29] E. V. Shuryak, Phys. Rev. D **52**, 5370 (1995).
[30] Compare the very similar discussion in the case of domain wall fermions in T. Blum *et al.*, Phys. Rev. D (to be published), hep-lat/0007038.
[31] D. Diakonov and V. Y. Petrov, Nucl. Phys. **B272**, 457 (1986).

[32] T. L. Ivanenko and J. W. Negele, Nucl. Phys. B (Proc. Suppl.) **63**, 504 (1998); R. C. Brower, T. L. Ivanenko, J. W. Negele, and K. N. Orginos, *ibid.* **53**, 547 (1997); T. L. Ivanenko, Ph.D. thesis, MIT, 1997.
[33] L. Venkataraman and G. Kilcup, hep-lat/9711006.
[34] F. R. Brown *et al.*, Phys. Rev. Lett. **67**, 1062 (1991).
[35] W. Bardeen, A. Duncan, E. Eichten, and H. Thacker, Phys. Rev. D **62**, 114505 (2000).
[36] T. DeGrand, A. Hasenfratz, and T. G. Kovacs, Phys. Lett. B **420**, 97 (1998).
[37] T. G. Kovacs, Phys. Rev. D **62**, 034502 (2000).
[38] K. G. Wilson, in *Erice 1975*, ''Proceedings, New Phenomena In Subnuclear Physics, Part A,'' New York, 1977, pp. 13–32; H. Kluberg-Stern, A. Morel, and B. Petersson, Phys. Lett. **114B**, 152 (1982).